Aggressive Mammary Cancers Lacking Lymphocytic Infiltration Arise in Irradiated Mice and Can Be Prevented by Dietary Intervention

Coral Omene[1], Lin Ma[2], Jade Moore[2], Haoxu Ouyang[3], Irineu Illa-Bochaca[3], William Chou[2], Manan S. Patel[3], Christopher Sebastiano[3], Sandra Demaria[3], Jian-Hua Mao[4], Kubra Karagoz[1], Michael L. Gatza[1], and Mary Helen Barcellos-Hoff[2]

ABSTRACT

Because the incidence of breast cancer increases decades after ionizing radiation exposure, aging has been implicated in the evolution of the tumor microenvironment and tumor progression. Here, we investigated radiation-induced carcinogenesis using a model in which the mammary glands of 10-month-old BALB/c mice were transplanted with *Trp53*-null mammary tissue 3 days after exposure to low doses of sparsely ionizing g-radiation or densely ionizing particle radiation. Mammary transplants in aged, irradiated hosts gave rise to significantly more tumors that grew more rapidly than those in sham-irradiated mice, with the most pronounced effects seen in mice irradiated with densely ionizing particle radiation. Tumor transcriptomes identified a characteristic immune signature of these aggressive cancers. Consistent with this, fast-growing tumors exhibited an immunosuppressive tumor microenvironment with few infiltrating lymphocytes, abundant immunosuppressive myeloid cells, and high COX-2 and TGFb. Only irradiated hosts gave rise to tumors lacking cytotoxic $CD8^{þ}$ lymphocytes (defined here as immune desert), which also occurred in younger irradiated hosts. These data suggest that host irradiation may promote immunosuppression. To test this, young chimera mice were fed chow containing a honeybee-derived compound with anti-inflammatory and immunomodulatory properties, caffeic acid phenethyl ester (CAPE). CAPE prevented the detrimental effects of host irradiation on tumor growth rate, immune signature, and immunosuppression. These data indicated that low-dose radiation, particularly densely ionizing exposure of aged mice, promoted more aggressive cancers by suppressing antitumor immunity. Dietary intervention with a nontoxic immunomodulatory agent could prevent systemic effects of radiation that fuel carcinogenesis, supporting the potential of this strategy for cancer prevention.

Introduction

The transformation of normal tissue into malignant cancer occurs under the influence of antitumor immunity and aging, both of which are key players in disease progression (1). Cancer evolution is also impacted by lifestyle, environment, and occupational exposures. In humans exposed to ionizing radiation, the period between exposure and increased risk of breast cancer is 30 to 40 years (2), hence host biology over decades likely modulates the evolution of biological features of a tumor that mediate its clinical behavior.

Radiation perturbs tissue homeostasis, in part, by activating inflam- matory processes that may not resolve, leading to a cycle of subclinical tissue damage and chronic, low-level inflammation (3, 4). Whereas one

[1]Rutgers Cancer Institute of New Jersey, Rutgers, The State University of New Jersey, New Brunswick, New Jersey. [2]University of California, San Francisco, San Francisco, California. [3]New York University School of Medicine, New York, New York. [4]Lawrence Berkeley National Laboratory, Berkeley, California.

Note: Supplementary data for this article are available at Cancer Immunology Research Online (http://cancerimmunolres.aacrjournals.org/).

C. Omene and L. Ma contributed equally to this article.

Current address for S. Demaria: Weill Cornell Medical College, New York, New York.

Corresponding Author: Mary Helen Barcellos-Hoff, Department of Radiation Oncology, University of California, San Francisco, 2340 Sutter Street, San Francisco, CA 94143. Phone: 415-476-8091; Fax: 415-476-9069; E-mail: MaryHelen.Barcellos-Hoff@ucsf.edu

body of work clearly establishes the capacity of chronic inflammation to initiate and promote cancer (4), other studies show that an intact immune system can prevent, control, and shape cancer by a process known as “cancer immunoediting” described by Mittal and collea- gues (5). Because immune cells eliminate aberrant cells, this process of editing shapes the developing cancer that can ultimately promote escape from immune control (6). Importantly, protumorigenic inflammation coexists with antitumor immunity, and interventions that alter the balance in favor of one can either accelerate or hinder tumor growth (4).

Data from human and experimental models support the idea that interaction between intrinsic factors, such as host biology, and extrin- sic conditions, including radiation exposure, significantly impact the biology of breast cancer. It is estimated that 8% of second primary cancers in the United States are associated with radiotherapy for first cancers in adults (7). Of concern are those who have been successfully treated with radiotherapy for childhood cancer. Women treated with radiation for a childhood cancer have a similar cumulative inci- dence of breast cancer by age 40 to that of women with *BRCA* gene mutations, and an incidence 10 to 20 times higher than the 1% cumulative incidence of general population (8). Compared with childhood cancer survivors who did not receive radiotherapy, girls treated with radiotherapy have a 2.9 times higher relative risk of subsequently developing breast cancer, which is greater than that of women who are *BRCA* mutation carriers (9). Moreover, child- hood radiation treatment is associated wth increased frequency of aggressive triple-negative breast cancer (TNBC) compared with age-matched, spontaneous cancer controls (10, 11).

Cancer incidence in humans increases exponentially with age, with 75% of newly diagnosed cases occurring in populations ages 55 years or older (https://www.cancer.gov/about-cancer/causes-prevention/risk/

age). Aging is associated with low levels of chronic inflammation that may contribute to age-associated diseases, including cancer. Likewise,

irradiation may increase inflammation. For example, serum IL6 increases both in older individuals (12) and atomic bomb survivors (13). Radiation exposure may also accelerate aging at some level (14).

Thus, modulating inflammation after irradiation is a prospective and achievable cancer prevention strategy in medically or occupationally irradiated populations that has not been tested.

We developed a radiation–genetic mammary chimera model to evaluate how carcinogenesis is affected by radiation-induced, non- mutational processes. Here, we examined the relationship between tumor microenvironment (TME) components and breast cancer phenotypes arising from *Trp53*-null mammary chimeras as a function of two factors, radiation type and host age. Densely ionizing radiation (DIR), which is present in the space radiation environment and used in radiation oncology, has potentially greater carcinogenic effect com- pared with sparsely ionizing radiation (SIR) that is prevalent on earth. Because occupational exposure (e.g., astronauts) and most radiother- apy occur in adults, here, we considered age at exposure as a factor. Here we show that, compared with our prior studies in 10-week-old mice (15), the effect of radiation quality was greater in aged mice (10 months old), demonstrating that DIR was more effective than SIR at inducing aggressive tumors. However, tumors arising in both DIR-and SIR-irradiated hosts were characterized by rapid growth rate and an immunosuppressive TME, both of which have been previously reported in young mice (15, 16). Only tumors arising in irradiated

mice were devoid of lymphocytic infiltrates, suggesting that nonmutational, radiation effects promoted immune evasion. This prompted us to use caffeic acid phenethyl ester (CAPE), the major

active component in propolis, a honeybee product that possesses

immunomodulatory (anti-inflammatory) and anticancer properties (17). CAPE adminis-tered postradiation in the diet of 10-week-old mice prevented estab- lishment of aggressive tumors with an

immunosuppressive TME. These studies suggest that systemic

inflammation and erosion of antitumor immunity elicited by radiation can be targeted after expo-sure to prevent aggressive tumors.

Materials and Methods

Animals

All animal experiments were performed at New York University School of Medicine (NYUSOM, New York, NY). The protocols for animal husbandry and experiments were conducted with institutional review and approval. Three-week-old BALB/c mice that served as hosts were purchased from Jackson Laboratory. Syngeneic *Trp53*$^{-/-}$

BALB/c mice were bred as described previously to 8 to 10 weeks of age

to provide donor mammary gland that was cryogenically preserved in 10% DMSO (16). All mice were housed 5 per cage, fed with Labdiet #5001 Rodent Formula (Purina Animal Nutrition LLC), and water *ad libitum*. The radiation-genetic chimera model was described previously in which the endogenous mammary epitheli- um of inguinal glands were surgically removed from 3-week-old wild-type BALB/c mice, the mice were aged

prior to irradiation, and the inguinal fatpads subsequently transplanted with the *Trp53*$^{-/-}$donor mammary fragments (15, 16).

For radiation quality experiments, mice aged to 10 months at

NYUSOM were transported to Brookhaven National Laboratory (Upton, NY), which conducted institutional review and approval. Mice were acclimated for at least 1 week, and whole-body irradiation was performed at the NASA Space Radiation Laboratory in Brookha- ven National Laboratory using a 5600 Curie (207 TBq) ^{137}Cs source to

deliver SIR to total body doses of 10, 50, or 100 cGy. Alternatively, mice were irradiated with DIR using 600 MeV/amu Fe, 350 MeV/amu Ar, and 350 MeV/amu Si ions at equivalent fluences (3 particles per 10^2 mm) in which total body average doses were calculated to be 80 cGy for Fe, 49 cGy for Ar, and 30 cGy for Si. Contemporaneous controls were transported, anesthetized, and sham-irradiated. Three days after irradiation, the cleared mammary fat pads of host mice were trans- planted with *Trp53*-null mammary gland fragments from nonirradi- ated donor mice. The approximately 1 mm^3 fragment was rapidly thawed from cryogenically preserved fragments of 8- to 10-week-old *Trp53*$^{-/-}$ mice inguinal glands. Mice were transported to NYUSOM and quarantined for 6 weeks upon return. Mice were monitored by palpation at weekly intervals before 6 months and twice weekly thereafter for 600 days posttransplantation.

For experiments using CAPE, BALB/c mice that served as hosts were purchased from Taconic Laboratory. The inguinal mammary glands of 3-week-old mice were cleared bilaterally of endogenous epithelium, as above. At 10 to 12 weeks old, the mice were irradiated with 100 cGy g-rays or sham-irradiated at NYUSOM. The cleared mammary fat pads of host mice were transplanted with *Trp53*-null mammary gland fragments from nonirradiated donor mice 3 days later. Sham or irradiated mice were then randomly assigned to receive *ad libitum*, either control diet (7012 meal) containing CAPE or control of 1% sucrose (Harlan Laboratories, Teklad lab animal diets). CAPE was added in sucrose at 10 g/kg as 10 nmol diet (CAPE at 0.47 mg/kg), 500 nmol (CAPE at 23.5 mg/kg), and 1,000 nmol diet (CAPE at 47 mg/kg). The CAPE concentration in the food and average food intake was used to estimate the dose. New 25-kg batches of diet were made every 3 months across the experiment. Blue or red food dyes at 0.2 g/kg diet were used to color code diets and prevent accidental feeding with the wrong diet. To preclude potential toxicity, dosing was escalated beginning with 10 nmol/ mouse/day from 4 weeks after transplant until 14 weeks, increased to 500 nmol at 26 weeks and ending at 1,000 nmol begun at 38 weeks, which was maintained for the remaining duration of the experiment. No toxicity (e.g., weight loss, poor grooming) was evident at any dose.

For all experiments, mice were palpated twice weekly from 6 months posttransplantation. Palpable tumors were measured twice a week using calipers. Tumors reaching 1 cm^3 were resected using survival surgery. The resected tumor was divided into four portions. One portion was frozen in liquid nitrogen for RNA extraction, one portion was embedded in optimum cutting tem- perature compound, one portion was formalin-fixed followed by paraffin embedding, and one portion was cut into fragments for viable preservation in DMEM (Gibco, #10564-011) with 10% FBS (Hyclone, #SH3007103) and 10% DMSO (Sigma, #D2650). Mice were further observed, and if the contralateral fat pad developed another tumor, then the tumor was monitored as above. If the resected tumor recurred, it was resected, and the mouse was euthanized. A gross necroscopy was performed upon termination. If no tumor developed from transplanted glands by the end of the experiment, mammary glands were collected, and the tissue stained by carmin alum (2 g carmin from Sigma #1022; 2.5 aluminum potassium sulfate from Sigma #A-7167; and 0.05g thymol crystals from Sigma #T-0501 in 500 mL distilled water). The stained wholemounts were evaluated to ascertain successful transplanta- tion. An informative transplant was defined as that which had an epithelial outgrowth evident by tumor development or >25% fat pad with gland development. Transplanted mammary glands that failed to develop epithelial outgrowths were censored.

Tumor growth rate analysis

Palpable tumors were measured twice weekly using calipers until reaching approximately 1 cm^3. Tumor volumes [V ¼ (4/3) × p × (W/2) x (W/2) x (L/2)] of individual *Trp53*-null tumors were calculated for each measurement, and the growth rate fitted as an exponential curve Y ¼ B e^{AX} using all measurements where Y is the tumor volume at day X, A is the slope of the growth curve, and B is the starting measure point of the tumor volume. To define fast versus slow tumor growth rate, the slopes of all tumor growth curves (n ¼ 33) were pooled and the top quartile was designated as fast growing (n ¼ 8) and the bottom quartile was designated as slow growing (n ¼ 8).

Immunofluorescence

Formalin-fixed paraffin-embedded (FFPE) sections were dewaxed and rehydrated. Antigen retrieval was performed by using Antigen Unmasking Solution (Vector Laboratories, #H-3300) according to the manufacturer's instructions. The slides were then washed once with PBS and blocked with 0.5% casein (Spectrum, #CA205)/PBS for 1 hour at room temperature. Slides were incu- bated overnight at 4°C with 100 mL primary antibody against the indicated antigen diluted in blocking buffer (0.5% casein/PBS) as indicated: estrogen receptor (NCL-ER-6F11, Novocastra; 1:50) diluted in Superblock Blocking Buffer (Pierce, #37515), cleaved caspase-3 (9661S, Cell Signaling Technology; 1:100), and COX-2 (ab15191, Abcam; 1:200). After washing with 0.1% Tween 20/PBS, slides were incubated for 1 hour at room temperature with 100 mL fluorochrome-conjugated secondary antibody dilutions (1:200 diluted in blocking buffer) of Alexa Fluor-488–conjugated Donkey anti-mouse (Invitrogen #A21202) for recognizing ER; Alexa Fluor-594–conjugated Donkey anti-rabbit (Invitrogen #A21207) for rec- ognizing cleaved-caspase 3 and COX-2. Nuclei were counterstained with 4^0, 6-diamidino-2-phenylindole (DAPI, 2 mg/mL; Molecular Probes). Sections were washed in PBS before mounting with VectaShield mounting medium (Vector Labs). Specimens were imaged using a 20x Zeiss Plan-Apochromat objective with 0.95 numerical aperture on a Zeiss Axiovert epifluorescent microscope. All images were acquired with a CCD Hamamatsu Photonics monochrome camera at 1392 × 1040-pixel size, 12 bits per pixel depth. All images were assembled as false-color images using the Metamorph imaging platform (Molecular Devices, Inc.). Allred scoring was used to determine ER status (18). Cleaved caspase-3 was counted manually by positive cells per high powered field (HPF), and the mean calculated by counting five nonoverlapping random HPF sections per tumor. COX-2 intensity per HPF was measured using Fiji-Image J (NIH, Bethesda, MD) scripts.

Some antigens were analyzed using 5-mm cryosections from tumors frozen in OCT (Sakura Tissue-Tek). Cryosections were fixed using 4% paraformaldehyde for 20 minutes at room temper- ature, specimens were blocked with 0.5% casein/PBS for 1 hour, and incubated with 100 mL anti-CD11b (ab75476, Abcam; 1:200) and anti-Gr1 (MAB1037, R&D Systems; 1:50) diluted in blocking buffer overnight at 4° C, followed by washes with 0.1% Tween 20/PBS and incubation with 100 mL Alexa Fluor-594 Donkey anti-rat (1:200; Invitrogen #A21209) and Alexa Fluor-488 Donkey-anti-rabbit (1:200; Invitrogen #A21206) secondary antibodies diluted in block- ing buffer for 1 hour at room temperature. Specimens were counter- stained with DAPI and washed in PBS before mounting with VectaShield mounting medium. Specimens were imaged as described above. $CD11b^bGr1^b$ double-positive cells were counted manually per HPF, and the mean calculated by counting five nonoverlapping random HPF sections per tumor.

Opal multiplex

FFPE sections were deparaffinized and rehydrated before antigen unmasking by Antigen Unmasking Solution (Vector Laboratories, #H- 3300 or #H-3301) according to manufacturer instructions. Endogenous peroxidase of each section was quenched by 100 mL 3% H_2O_2 in PBS (diluted from 30% H_2O_2, Sigma #H1009) for 15 minutes and washed twice with TN buffer (0.1 mol/L Tris-HCl, 0.15 mol/L NaCl). The Opal 6-color kit (NEL796001KT, PerkinElmer) and Opal 7-color kit (NEL811001KT, PerkinElmer) were used. Each section passed through five or six sequential rounds of staining. Each round consisted of a protein block with 0.5% casein in TN buffer for 1 hour at room temperature, a primary antibody overnight incubation at 4°C, a corresponding secondary horseradish peroxidase (HRP)–conjugated polymer incubation for 1 hour at room temperature, and a 10-minute incubation for each HRP-conjugated polymer, which mediated the covalent binding of a different fluorophore using tyramide signal amplification (all primary and secondary antibodies listed in Table 1). An additional antigen retrieval using heated citric acid buffer (pH 6.0) for 15 minutes was then used to remove bound antibodies before the next step in the sequence. After all sequential reactions, sections were counterstained with spectrum appropriate DAPI (NEL796001KT or NEL811001KT, PerkinElmer) and mounted with Vectashield Hard Set mounting medium (H-1400, VectaShield). Opal-stained sections were imaged using the Vectra Multispectral Imaging System version 2 (PerkinElmer). Images were analyzed by inForm 2.1 (PerkinElmer). Single stained slides for each marker and associated fluorophore were used to establish the spectral library, which helped to separate the individual marker from the multiplexing image cube. For each marker, positive cells were determined on the basis of the mean fluorescent intensity per case. The inForm 2.1 (PerkinElmer) trainable tissue segmentation algorithm (PerkinElmer) was used to segment tumor and stromal regions based on the markers and DAPI-stained nuclear shape. The percentage of positive cells for each marker in the region-designated tumor or stroma was analyzed separately by the score algorithm (PerkinElmer) in 10 random images at 20x magnification.

Lymphocyte infiltrate pattern analysis

FFPE tumor sections were stained by CD8 (Table 1) as the method indicated above (Opal) and scanned using the Vectra system (PerkinElmer). The images of the whole sections were used for pattern analysis. The $CD8^{þ}$ T-cell infiltration into tumors was classified into three patterns: infiltrated, excluded, or desert. We defined infiltrated tumors as those with dense $CD8^{þ}$ cells that were well distributed across the tumor; excluded tumors were characterized by a dense accumu- lation of $CD8^{þ}$ cells at the tumor edge; and desert tumors contained few $CD8^{þ}$ cells. Tumor sections were evaluated by two observers blind to the experimental group.

Gene expression profiling

Frozen tumor tissues (50 mg) were lysed in 1 mL TRIzol reagent and homogenized with Omni Tissue Homogenizer on medium setting for 30 seconds, then incubated 3 minutes in 0.2 mL chloroform, followed by centrifuging for 15 minutes at 12,000 *g* at 4°C. The aqueous phase was transferred to a new tube and 0.5 mL isopropanol was added for 10 minutes. Samples were then centrifuged for 10 minutes at 12,000 *g* at 4°C. The supernatant was discarded, and the white gel-like pellets were resuspended in 1 mL of 75 % ethanol. The samples were then vortexed briefly, then centrifuged for 5 minutes at 7,500 *g* at 4°C. The supernatant was discarded, and the RNA pellet airdried for 5 to 10 minutes before resuspending in 30 mL of RNase-free water. The

Table 1. Antibodies for Opal staining.

First antibody	Second antibody	Opal dye
Set 1 Ly6G (60031, Stem Cell Technology)	Goat-anti-rat HRP (31470, Thermo Fisher Scientific)	Opal 520 (NEL796001KT, PerkinElmer) Set 1 Foxp3 (14-5773-82, eBioscience)	Goat-anti-rat HRP (31470, Thermo Fisher Scientific)	Opal 540 (NEL796001KT, PerkinElmer) Set 1 CD4 (14-9766, eBioscience)	Goat-anti-rat HRP (31470, Thermo Fisher Scientific)	Opal 570 (NEL796001KT, PerkinElmer) Set 1 CD11b (ab133357, Abcam)	Goat-anti-rabbit HRP (31466, Invitrogen)	Opal 620 (NEL796001KT, PerkinElmer) Set 1 CD45 (ab10588, Abcam)	Goat-anti-rabbit HRP (31466, Invitrogen)	Opal 690 (NEL796001KT, PerkinElmer Set 1 DAPI	Spectrum DAPI (NEL796001KT, PerkinElmer)
Set 2 CD8 (ab203035, Abcam)	Goat-anti-rabbit HRP (31466, Invitrogen)	Opal 520 (NEL796001KT, PerkinElmer) Set 2 Ki67 (RM9106-S1, Thermo Fisher Scientific)	Goat-anti-rabbit HRP (31466, Invitrogen)	Opal 540 (NEL796001KT, PerkinElmer) Set 2 CD4 (14-9766, eBioscience)	Goat-anti-rat HRP (31470, Thermo Fisher Scientific)	Opal 570 (NEL796001KT, PerkinElmer) Set 2 CD3 (MA514524, Thermo Fisher Scientific)	Goat-anti-rabbit HRP (31466, Invitrogen)	Opal 620 (NEL796001KT, PerkinElmer) Set 2 Pan-Cytokeratin (ab9377, Abcam)	Goat-anti-rabbit HRP (31466, Invitrogen)	Opal 690 (NEL796001KT, PerkinElmer) Set 2 DAPI	Spectrum DAPI (NEL796001KT, PerkinElmer)
Set 3 Gr1 (RB6-8C5; ab25377, Abcam)	Goat-anti-rat HRP (31470, Thermo Fisher Scientific)	Opal 520 (NEL811001KT, PerkinElmer)
Set 3 p-SMAD2 (44-244G, Thermo Fisher Scientific)	Goat-anti-rabbit HRP (31466, Invitrogen)	Opal 540 (NEL811001KT, PerkinElmer)
Set 3 TGFb (AF-101-NA, R&D Systems)	Goat-anti-chicken HRP (ab6877, Abcam)	Opal 570 (NEL811001KT, PerkinElmer) Set 3 CD8 (ab203035, Abcam)	Goat-anti-rabbit HRP (31466, Invitrogen)	Opal 620 (NEL811001KT, PerkinElmer) Set 3 CD11b (ab133357, Abcam)	Goat-anti-rabbit HRP (31466, Invitrogen)	Opal 650 (NEL811001KT, PerkinElmer) Set 3 Pan-Cytokeratin (ab9377, Abcam)	Goat-anti-rabbit HRP (31466, Invitrogen)	Opal 690 (NEL811001KT, PerkinElmer) Set 3 DAPI	Spectrum DAPI (NEL811001KT, PerkinElmer)
Set 4 CD33 (NBP2-37388, Novus Biologicals)	Opal Polymer HRP Ms + Rb (ARH1001EA, PerkinElmer)	Opal 520 (NEL811001KT, PerkinElmer)
Set 4 p-SMAD2 (44-244G, Thermo Fisher Scientific)	Goat-anti-rabbit HRP (31466, Invitrogen)	Opal 540 (NEL811001KT, PerkinElmer)
Set 4 TGFb 1D11 (BP0057, Bio X Cell)	Goat-anti-Ms IgG1 HRP (ab97240, Abcam)	Opal 570 (NEL811001KT, PerkinElmer) Set 4 CD11b (ab133357, Abcam)	Goat-anti-rabbit HRP (31466, Invitrogen)	Opal 620 (NEL811001KT, PerkinElmer) Set 4 COX2 (ab15191, Abcam)	Goat-anti-rabbit HRP (31466, Invitrogen)	Opal 650 (NEL811001KT, PerkinElmer) Set 4 PD-L1 (ab20592, Abcam)	Goat-anti-rabbit HRP (31466, Invitrogen)	Opal 690 (NEL811001KT, PerkinElmer) Set 4 DAPI	Spectrum DAPI (NEL811001KT, PerkinElmer)

samples were incubated in a heat block at 60°C for 15 minutes before determining total RNA quality (RIN > 7.0), and quantity was determined using an Agilent 2100 Bioanalyzer and Nanodrop ND-100. The Affymetrix mouse Genechip 2.0 ST arrays were used according to manufacturer's protocol (Thermo Fisher Scientific, #902119) for tumors from aged (10-month-old) mice. Gene expres- sion data is archived in Gene Expression Omnibus (GEO) under accession number GSE126769. The raw data was background adjusted and quantile-normalized using the Robust Multichip Average (RMA) algorithm from the Bioconductor package oligo (19). Read and mapping quality was analyzed using R package affyQCReport (20). Analyses were performed using BRB-ArrayTools developed by Dr. Richard Simon and the BRB-ArrayTools Devel- opment Team (21). Intrinsic subtyping was completed using the PAM50 method developed by Perou and colleagues at the University of North Carolina at Chapel Hill (Chapel Hill, NC; ref. 22). Express RNA sequencing (RNA-seq) was performed on tumors derived from CAPE- and control-treated, irradiated hosts using the TruSeq RNA Sample Preparation Guide Protocol by Illumina (#15008136 A). Raw sequencing data were received in FASTQ format. Read mapping was performed using Tophat 2.0.9 against the mm10 human reference genome (23). The resulting BAM alignment files were processed using the HTSeq 0.6.1 python framework and respective mm10 GTF gene annotation, obtained from the University of California, Santa Cruz (UCSC) database. Subsequently, the Bioconductor package

DESeq2 (3.2) was used to identify differentially expressed genes (DEG; ref. 24). This package provides statistics for determination of DEGs using a model based on the negative binomial distribution. Gene expression data from RNA-seq data are archived on GEO under accession number GSE128930. For both the microarray and RNA-seq data, statistically significant genes were determined using the Benjamini–Hochberg method for controlling false discovery rate (FDR). Genes with an $P_{adj} < 0.05$ were determined to be differentially expressed.

Gene clustering was done using a Pearson correlation coefficient (PCC). Pathway analysis and subsequent predictions in each tissue were defined using the statistically significant genes with a fold change

1.2 or (–1.2) comparing treated versus sham ::: S controls. Gene set enrichment analysis (GSEA) using the Molecular Signatures Data- base's (MSigDB) eight major collections of gene sets (i.e., H and C1– C7; ref. 25) with an FDR < 0.05 from the entire list of genes was performed. A Web-based gene set analysis toolkit (WebGestalt) was used to complete functional enrichment and pathway analysis of significant genes across treatments (26, 27). All heatmaps were generated using ggplot2 package available through R.

The mean expression of gene expression signatures of specific aspects of immune cell signaling was calculated for each sample (n 23) as ¼ reported previously (28–32). The Student t test was used to assess pathway scores between treatment groups. Tumors from sham, CAPE, IR, and IR þ CAPE-treated animals were compared

using a panel of 18 gene expression signatures; red indicates high signature score (relative to dataset median) while blue corresponds with low relative score. Assessments of human TNBC subtypes of *Trp53*-null tumors were assigned using the TNBC subtype tool (33).

Statistical analysis

To compare growth rate between IR and sham groups, each growth curve was fitted as an exponential curve to extrapolate tumor size for a period representing the 30 days, as reported previously (16). *R* values of >0.9 indicated that this was a reliable representation of the growth trajectory, therefore, tumor sizes in a treatment group were averaged every day for 30 days, independent of when the tumor arose, to permit comparison of growth rates between treatment groups. The growth rate of tumors within a treatment group was compared by averaging these normalized growth curves. The statistical analysis for all exper- imental data was performed using Prism 7 (GraphPad) and IBM SPSS Statistics. Differences between treatment groups were determined using Student *t* test or Mann–Whitney test as indicated. PCC was used to test correlation between two components (IBM SPSS). A statistically significant difference was considered when *P* value was smaller than 0.05.

Results

Host age and radiation quality affect the frequency and spectrum of *Trp53*-null carcinomas

The radiation-genetic mammary chimera model separates nonmu- tational radiation effects and host biology, like age, that can influence cancer development. After the mice with cleared mammary fat pads were aged to 10 months, which is roughly equivalent to a 45-year-old human, they were irradiated and 3 days later, they were transplanted with nonirradiated *Trp53*-null mammary epithelium (ref. 34; Fig. 1A). We observed that only 50% of *Trp53* transplants generated outgrowths in aged mice, which is in contrast to our previous observation of 90% outgrowth efficiency in 10-week-old mice (15, 16), which is likely due to ovarian hormone decline. The reduced number of informative fat pads precluded statistically meaningful evaluation of radiation dose dependence. Therefore, mice were grouped according to radiation quality (i.e., SIR vs. DIR) for comparison with sham-irradiated mice. The mean time to a palpable tumor was not affected by host irradiation (358 99 days for sham-hosts, *n* 7; 366 64 days for SIR-irradiated hosts, *n* 18; 353 76 days for DIR-irradiated hosts, *n* 27). However, the frequency of tumors arising from transplants in irradiated hosts was significantly increased compared with transplants

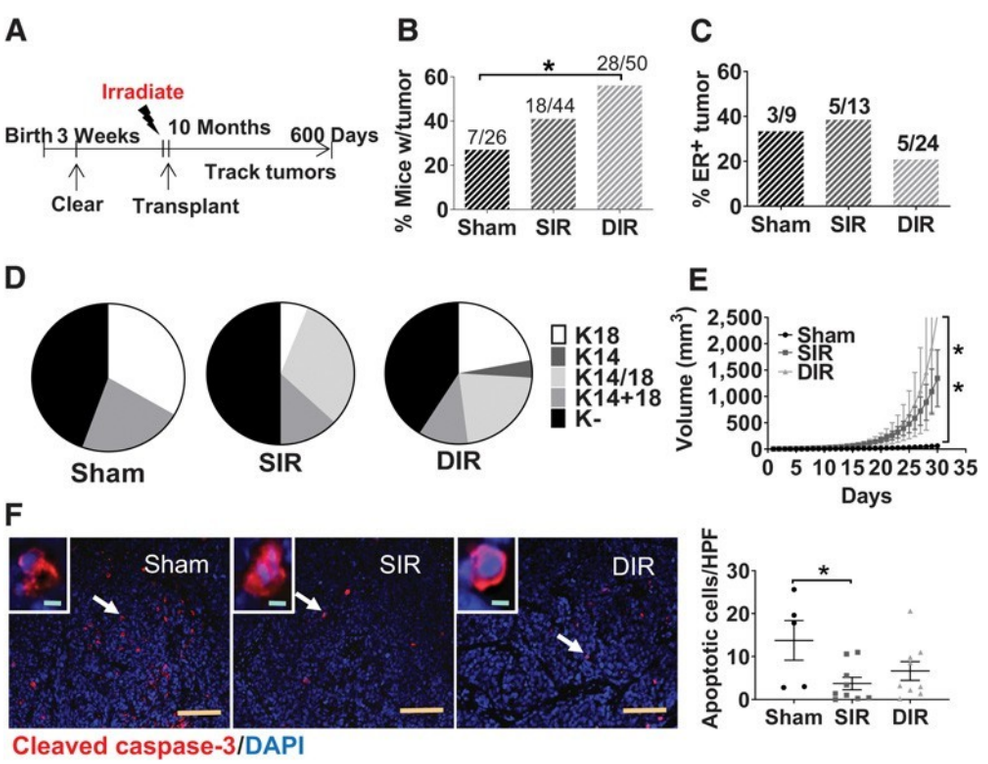

Figure 1.
Tumor characteristics as a function of host irradiation at 10 months of age. A, Experimental scheme. The endogenous epithelium of the inguinal mammary glands of 3-week-old mice were surgically removed. Mice were aged until 10 months old, whole-body irradiated with SIR or DIR, and 3 days after irradiation, subsequently transplanted with *Trp53*-null mammary fragments. Mice were monitored for tumorigenesis for approximately 600 days. B, Frequency of tumors arising in aged hosts (corrected for outgrowth efficiency). , $P <$ 0.05, x^2. Numbers above columns represent mice with tumors over total mice in that group. C, The frequency of ER^b tumors as a function of aged host irradiation. Numbers above columns represent ER^b tumors over total tumors in that group. D, The keratin staining of tumors arising in sham-irradiated (n 9), SIR-irradiated (n 16), and DIR-irradiated (N 27) hosts. E, Tumor growth rate over 30 days following detection by palpation for each group of aged mice. Mean SEM. Sham: n 6; SIR: n 13; DIR: n 20; , $P <$ 0.01; one-way ANOVA. F, Left, representative images of apoptotic cells marked by cleaved caspase-3. White arrows indicate zoomed cells in the image. Tan scale bars, 100 mm; green scale bars, 5 mm. Right, quantitation of apoptotic cell density in tumors arising in SIR-irradiated (n 9) or DIR-irradiated (n 9) hosts compared with tumors in sham group (n 5). Data are the mean SEM; , $P <$

0.05; Student *t* test.

in sham-irradiated contemporaneous controls ($P < 0.05$, x^2; Fig. 1B). Host irradiation with DIR was more effective than SIR in promoting tumorigenesis. Tumors arose from 20% of informative transplant outgrowths in sham-irradiated mice, 40% in mice exposed to SIR, and nearly 60% in mice exposed to DIR (Fig. 1B). Compared with our prior studies in mice irradiated at 10 weeks old (15, 16, 35), the differential between sham and irradiated hosts at 10 months was greater, as was the differential between SIR and DIR.

The murine mammary gland consists of two major cell types, basal myoepithelial cells that express keratin 14 (K14) and p63, and luminal cells that express keratin 8/18 (K18) and estrogen receptor (ER). Most (60%) cancers arising from *Trp53*-null outgrowths in young mice (10 weeks at transplant) are ER-positive, which host irradiation decreases (16, 36). Compared with young mice, fewer (33%, 3/9) ER-positive cancers arose in aged, sham-irradiated mice. The frequen- cy was similar (39%, 5/13) for tumors arising in SIR-irradiated aged hosts but was decreased in DIR-irradiated mice (21%, 5/24; Fig. 1C). In young mice, most *Trp53*-null tumors arising in sham-irradiated hosts exhibit a pseudoglandular pattern consisting of K14- and K18- positive cells, whereas both SIR and DIR host irradiation favors K18 tumors (15). In aged mice, nearly half of the tumors were negative for both keratins (Fig. 1D). Compared with tumors arising in sham- irradiated aged hosts, SIR or DIR host irradiation favored development of pseudo-glandular tumors (i.e., K14/K18) at the expense of K18 tumors. These data extend our prior work showing that SIR and DIR exposure affects the tumor spectrum arising from nonirradiated *Trp53*-null epithelium (29).

Host irradiation leads to rapid growth of subsequent tumors

The growth rate of individual *Trp53*-null tumors is heterogeneous, but tumors arising in irradiated young mice consistently grow faster, regardless of latency (15, 16, 35, 36). To permit comparison among tumors, each growth curve within a treatment group was fitted as an exponential curve, which was used to extrapolate tumor size for a period of 30 days postdetection, independent of when the tumor arose. The growth rate of tumors arising in aged mice irradiated with either SIR or DIR was significantly faster than tumors arising in aged, sham-irradiated mice (P 0.003; Fig. 1E). Because we previously reported this phenotype in young irradiated mice (15, 16), the data suggest that rapid growth rate is a consequence of host irradiation rather than host age *per se*, although older age appears to exacerbate the effect of host irradiation.

Tumor growth rate is the sum of cell production and loss. Tumor cell mitotic rate was not different between treatment groups (23 ± 3 for sham hosts, n ¼ 9; 25 ± 6 for SIR hosts, n ¼ 16; 23 ± 2, n ¼ 26 for DIR hosts), nor was proliferation rate as marked by Ki67 (20% ± 4% for sham hosts, n ¼ 8; 16% ± 3% for SIR hosts, n ¼ 7; 16% ± 3%, n ¼ 13 for DIR hosts). We next tested cell loss using cleaved caspase-3, a marker of apoptotic cells. Apoptosis was significantly greater in tumors arising in sham-irradiated versus irradiated hosts (P ¼ 0.02; Fig. 1F).

Tumors arising in irradiated host exhibit distinct expression signatures

To explore how host irradiation globally impacted tumor features that mediate growth, we used an Affymetrix Genechip Mouse Gene 2.0 ST platform to profile RNA of 43 tumors arising in sham (n ¼ 9), SIR-irradiated (n 15), and DIR-irradiated (n 19), aged mice. Of these, 32 tumors were ER-negative and 11 were ER-positive. Mam- mary cancers arising from *Trp53*-null epithelium are genomically heterogeneous in a manner that reflects the diversity of human breast cancers (35, 37, 38). Using PAM50-based molecular subtyping (22), we

assessed the distribution of intrinsic breast cancer subtypes (Supple- mentary Fig. S1A). The overall subtype distribution was 42% luminal A (18/43), 21% luminal B (9/43), 12% HER2-enriched (5/43), 16% basal- like (7/43), and 9% normal-like (4/43) (Supplementary Fig. S1B). Among ER-positive tumors, 45% were categorized as luminal A by PAM50 (Supplementary Fig. S1C). The spectrum of PAM50-intrinsic subtypes was significantly affected by DIR host irradiation but not by SIR host irradiation ($P < 0.05$, ANOVA).

Unsupervised hierarchical clustering (UHC) of all genes identified

three tumor clades distinguished by five major gene clusters (Fig. 2A). Group 1 (G1) was composed of nine tumors arising only in irradiated hosts, the majority of which (6/9) were from DIR-exposed mice. Group 2 (G2; *n* 16) contained mostly (6/9) tumors arising in sham- irradiated mice. Group 3 (G3; *n* 18) was composed of tumors from all treatments, but most were (8/15) tumors arising in SIR-irradiated hosts. Tumor ER status did not appear to be a factor, as it was distributed across groups. The five major gene clusters were charac- terized by gene set enrichment analysis (25). These clusters represented significant differences among tumors and showed downregulation of genes associated with mammary stem cells (cluster 1), immune system processes (cluster 2), cellular response to external stimulus (cluster 3), and epithelial-to-mesenchymal transition and TGFb (cluster 4). A set of genes was also upregulated in mammary stem cells (cluster 5; Supplementary Table S1). These processes were similar to those we identified for tumors arising in young, irradiated mice (15, 16, 36).

G1 expression profile patterns were the most distinctive. Two clusters of genes associated with mammary stem cells were low in G1 tumors compared with tumors in G2 and G3. G1 tumors were also characterized by genes decreased upon loss of E-cadherin, which promotes metastasis (39), and is caused by TGFb activation, partic- ularly in irradiated cells (40). Both G2 and G3 tumor expression profile patterns were more heterogeneous than G1 tumors. The G2 group was characterized by high expression of mammary stem cell genes, whereas G3 group expressed genes decreased in mammary stem cells, as well as genes associated with TGFb. G1 tumors were characterized by *BMP2* activity, which is reported to affect progesterone receptor signaling and induction of prostaglandin synthase (41).

G1, which consisted entirely of tumors arising in irradiated mice, exhibited high expression of cluster 2 implicated in immune system processes, which was further refined as three minor gene clusters that implicated discrete immune processes: leukocyte traf- ficking ($P < 0.05$), apoptosis-related ($P < 0.05$), and inflammatory processes ($P > 0.001$; Fig. 2B). In contrast, G2, which was enriched in tumors arising in sham-irradiated mice, exhibited low expression of gene cluster 2, whereas G3 tumors exhibited an intermediate pattern–genes associated with leukocyte trafficking and inflamma- tory processes were elevated but apoptosis-related activities were reduced compared with G1.

Specific genes were enriched in G1 tumors compared with tumors in G2 and G3 (Supplementary Table S2). Leukocyte endogenous med- iators included a 17-fold increase in *Il1b*, as well as antiapoptotic *Xiap (*x-linked inhibitor of apoptosis protein) and *Bir (Baculovirus* inhibitor of apoptosis protein repeat). Key proinflammatory mediators included a 16-fold change in *Ptgs2,* which encodes COX2. Expression of *Ptgs2* was significantly elevated in tumors arising in irradiated hosts (Fig. 3A). Thus, programs important in immunity and inflammation distinguished tumors arising in irradiated hosts from those arising in sham-irradiated hosts.

To further test this idea, we then conducted supervised comparison of ER-negative tumors using 725 cluster 2 genes implicated in immune functions (Supplementary Table S3). Expression profiling of tumors

¼ ¼

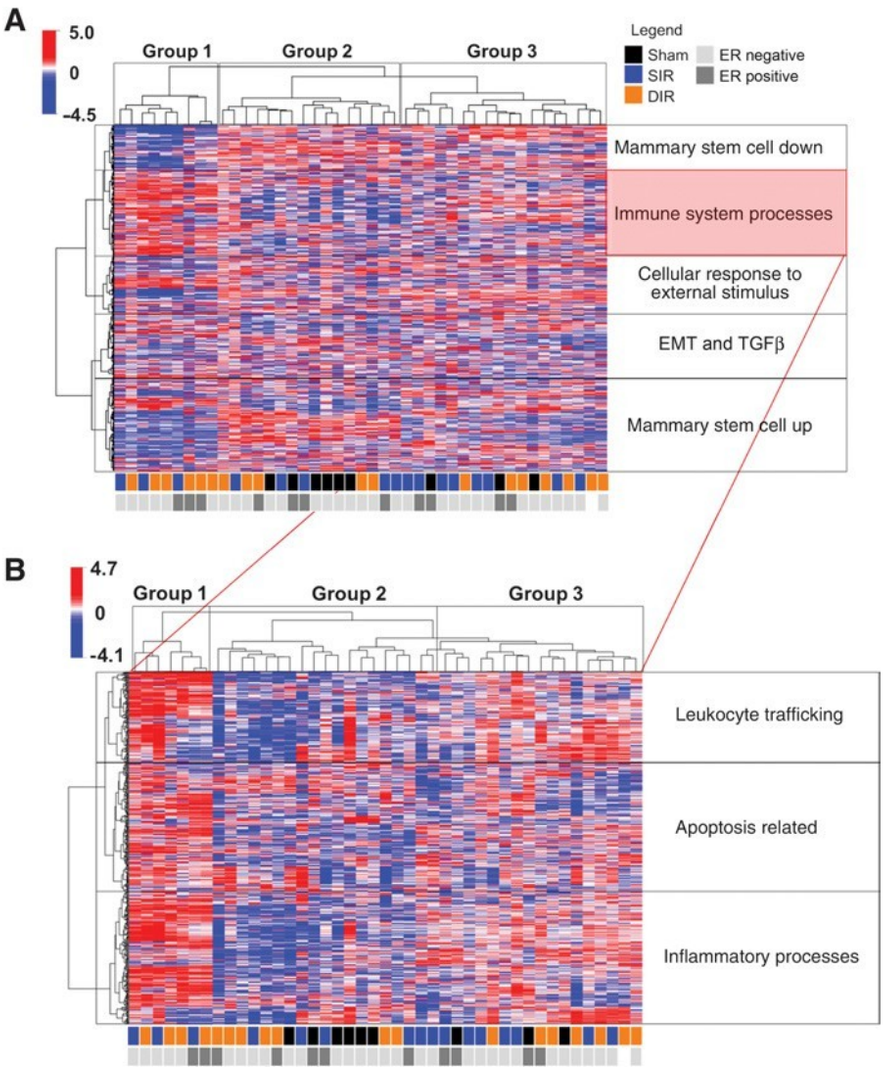

Figure 2.
Tumors arising in aged, irradiated hosts evoke important programs implicated in immunity and inflammation. A, UHC of gene expression determined using an Affy- metrix Genechip Mouse Gene 2.0 ST to profile 43 tumors (light gray ER¼*n* 32; dark gray ER^{b}, *n* 11) arising in sham (black, *n* 9), SIR-irradiated (blue, *n* 15), and DIR-irradiated (orange, *n* 19), aged mice. Five major gene clusters indi- cated. B, Expression profiling of tumors arising in irradiated hosts. Enlarged view of gene cluster 2 (immune system process- es) and the three indicated associated minor gene clusters.

arising in irradiated versus sham-irradiated hosts indicated that genes

involved in inflammatory and immune response (21 genes), extracel- lular matrix disassembly (18 genes), and immune cell trafficking (32 genes) were the top-ranked ($P > 0.001$) processes that distinguished tumors from irradiated, aged mice from sham-irradiated mice. Among

the 15 most significant upstream regulators identified by The Database for Annotation, Visualization, and Integrated Discovery (DAVID)

ranked by z-score ($P < 0.05$), the majority were proinflammatory factors, including IL4, IL4 receptor, IL1b, and TGFb. Our previous work showed that TGFb is a critical signal in the irradiated host (16, 36, 38).

Among the top ranked upregulated molecules were COX-2 and

granzyme D. We sought to confirm *Ptgs2* gene expression, whose product is COX-2, by assessing COX-2 protein via immunofluo- rescence (Fig. 3B). Tumors from irradiated hosts exhibited increased COX-2 immunostaining compared with tumors from sham-irradiated mice. COX-2 promotes the immunosuppressive activity of myeloid-derived suppressor cells and tumorigenesis (42). Thus, we sought validation of COX-2 activity by enumerating CD11b^{b}Gr1^{b} cells, which were increased in tumors from irradi- ated host (Fig. 3C). These cells bore the markers of suppressive

myeloid cells, some of which might harbor suppressive activity, and could also reflect neutrophils that are known to be suppressive in some contexts. Further phenotypic experiments are needed to determine whether this population is functionally immunosup- pressive. The frequency of $CD11b^{þ}Gr1^{þ}$ cells was positively cor- related with COX-2 intensity (PCC r 0.48, $P < 0.05$; Fig. 3D). ¼ Together, with the accelerated growth rate, these data led us to investigate the tumor immune infiltrate as a function of host irradiation.

The pattern of immune infiltrates of tumors arising in irradiated, aged mice is distinct

Inflamed tumors exhibit preexisting immunity, as evidenced by an abundance of tumor-infiltrating lymphocytes (TIL) and expression of checkpoint markers including PD-L1. Tumors that exclude T cells often exhibit immunosuppressive immune cells, reactive stroma, and angiogenesis. A third class of tumors are devoid of significant T-cell infiltrate, that is, deserts, which are generally genomically stable and proliferative (43). We classified tumors according to $CD8^{þ}$ TIL patterns (Fig. 4A). Tumors arising in sham-irradiated mice (n ¼ 8) were either infiltrated (63%) or excluded (37%). In contrast, 28% (n ¼

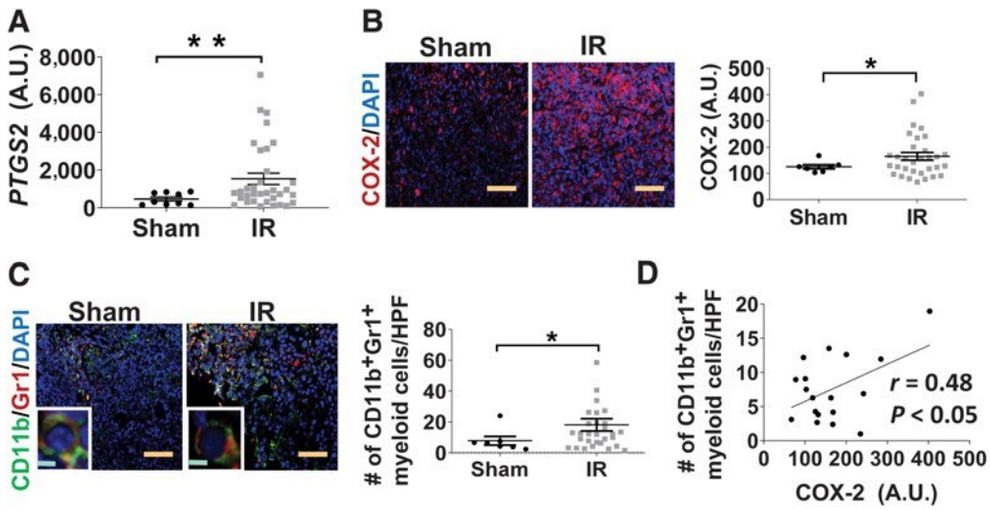

Figure 3.

An immunosuppressive TME is prominent in tumors arising in irradiated mice. A, Expression of *PTGS2* (COX-2) measured by the Affymetrix GeneChip Mouse 2.0ST platform. Sham: *n* 9; irradiated (IR): *n* 34. Data showed the mean SEM; *P* values were determined by Mann–Whitney test. , $P < 0.01$. B, Quantification of COX-2 expression by immunofluorescence staining with representative images. Sham: *n* 7; IR: *n* 32. , $P < 0.05$ by Student *t* test (bars, mean SEM). Tan scale bars, 100 mm. C, Left, representative images from immunofluorescence staining against CD11b and Gr1. Left corners are zoomed positive cells in the image. Tan scale bars, 100 mm; green scale bars, 5 mm. Right, quantitation of $CD11b^{b}Gr1^{b}$ cells per HPF (Sham: $n = 7$; IR: $n = 30$). , $P < 0.05$ by Student *t* test (bars, mean ± SEM). D, Correlation between $CD11b^{b}Gr1^{b}$ cells and COX-2 intensity per HPF. Each point is one tumor ($n = 18$). $P < 0.05$ was determined by PCC, $r = 0.48$.

43) of tumors arising in irradiated mice were deserts. Quantitative analysis using InForm software to enumerate the percentage of $CD8^{b}$ T cells in tumor versus stroma showed that $CD8^{b}$ T-cell frequency in the tumor, but not the stroma, was significantly lower in tumors from irradiated hosts (Fig. 4B).

Tumor cell apoptosis from cytotoxic T-cell activation can limit tumor growth by both direct and indirect mechanisms (44). Consistent with functional, though ineffective, antitumor immunity, the frequen- cy of $CD8^{b}$ TILs negatively correlated with tumor growth rate (Fig. 4C) and COX-2 expression (Fig. 4D). To facilitate analysis of the biology associated with tumor growth rate, tumors (n 33) were divided into quartiles based on growth. The top quartile was desig- nated as fast growing (n 8), and the bottom quartile was designated as slow growing (n 8). More tumors in the fast-growing group were deserts or excluded than in the slow-growing group (Fig. 4E). Exclu- sion of lymphocytes is often accompanied by high prevalence of myeloid cells (45, 46). We found that the frequency of $CD11b^{b}Ly6G^{b}$ cells was greater in fast-growing tumors (Fig. 4F) and positively correlated with growth rate across all tumors (Fig. 4G). Ineffective antitumor immunity could also be due to PD-L1 expression (47), and COX-2 regulates PD-L1 expression in tumor-associated macro- phages (48). Consistent with this, PD-L1 expression was increased in fast-growing tumors (Fig. 4H).

We next considered the TGFb gene signature that characterized tumors arising in the irradiated, aged host. Radiation induces acute TGFb activation, whose effects are persistent (16, 36). TGFb is known for its ability to suppress lytic activity of $CD8^{b}$ T-cell function (45) and is a key signal that promotes immunosuppressive myeloid differen- tiation and their efficacy in suppressing cytolytic lymphocytes (49). Hence, we evaluated immunostaining of active TGFb (Fig. 4I) and phosphorylation of SMAD2 (pSMAD2), the downstream target of TGFb receptor kinase (Fig. 4J), which were both significantly increased in fast-growing tumors, consistent with a role of TGFb as a key component of the immunosuppressive TME. Together, unsu-

pervised genomic analysis and validation immunostaining indicated that host irradiation promoted tumors with an immunosuppressive TME in which high TGFb and pronounced myeloid infiltration likely leads to exclusion of $CD8^{b}$ lymphocytes and aggressive tumor behavior.

Dietary CAPE prevents the irradiated host tumor phenotype

Advanced host age at irradiation increased *Trp53*-null tumor frequency, but rapid tumor growth rate is also observed in *Trp53*- null carcinomas arising in young (10-week) irradiated hosts (15, 16, 35, 36). Both radiation and aging are associated with decreased immunity and increased inflammation (13, 50). To test whether modulating inflammation early in carcinogenesis affected the tumor type that developed, we conducted experiments with young mice. Mammary glands were cleared at 3 weeks, mice were irradiated (100 cGy g-radiation) at 10 weeks and were transplanted with *Trp53*-null mammary fragments 3 days later (Fig. 5A). Mice were randomized 30 days later to chow containing CAPE, a nontoxic, anti-inflammatory compound (major active component of honeybee propolis) that has demonstrated anticancer and immunomodulatory properties (17). We chose CAPE primarily because of its natural favorable toxicity profile, which makes it an attractive potential treatment in humans, and because our work using CAPE demonstrates its antiproliferative effects on breast cancer (51, 52).

The time course of tumor detection was statistically different ($P <$ 0.01) among irradiated hosts compared to sham-irradiated hosts (Fig. 5B). Similar to the effect of aged host irradiation on tumor growth rate described above (Fig. 1), tumors arising in young, irradiated, control chow–fed hosts grew significantly faster than those arising in sham-irradiated hosts (Fig. 5C). Tumors arising in CAPE- fed mice exhibited a growth rate similar to sham-irradiated mice on control diet (Fig. 5C). The pattern of $CD8^{b}$ TILs from tumors arising irradiated, control chow–fed mice were similar to aged mice and included 30% classified as deserts (Fig. 5D). In contrast, tumors from

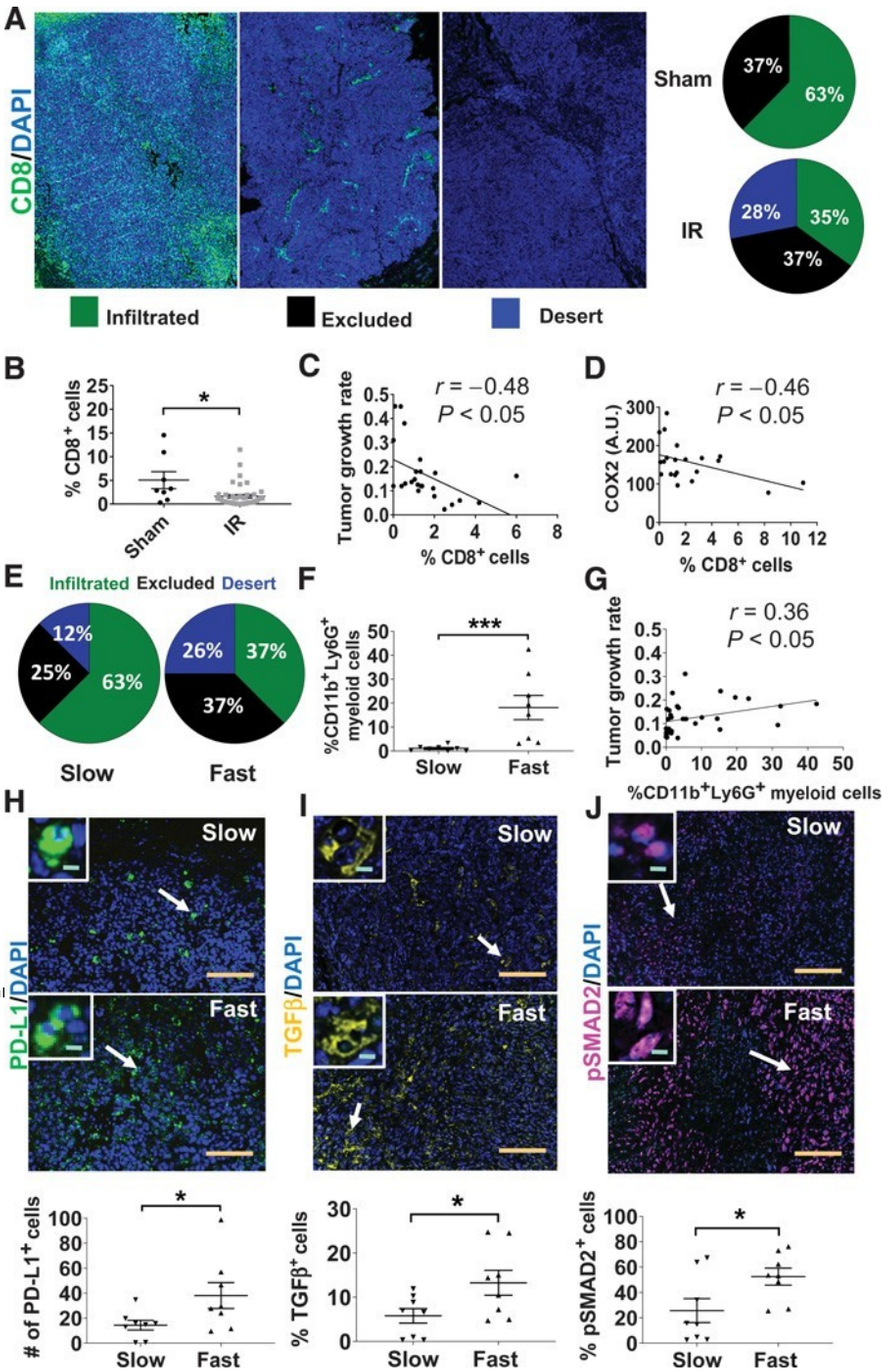

Figure 4.

Patterns of CD8^{b} lymphocytic infiltration associate with tumor growth rate. A, Left, representative images of *Trp*53-null mouse mammary gland tumors that were stained with anti-CD8 (green) and DAPI (blue) and scanned using the Vectra system. Right, tumors were classified by three independent observers as inflamed (green), excluded (black), or desert (blue) as described in Materials and Methods. The proportion of tumor types as a function of host irradiation are shown for sham (n 8) and irradiated (IR, n 43) hosts. B, The proportion of CD8^{b} cells within the tumor region of tumors from the sham (n 8) and IR groups (n 43). , $P < 0.05$ by Mann–Whitney test (bars, mean SEM). C, Correlation between the proportion of CD8^{b} cells within the tumor region and tumor growth rate (n 24; sham, n 4; IR, n 20). PCC r -0.48, $P <$ 0.05.

D, Correlation between the proportion of CD8^{b} within the tumor region and COX-2 mean intensity. n 21; sham, n 5; IR, n 16). PCC r − 0.46, $P < 0.05$. E, The immune infiltrate status of the bottom (i.e., slow, 8) and top (i.e., fast, n 8) quartile based on growth rate. Inflamed, green; excluded, black; desert, blue. F, The proportion of CD11b^{b}Ly6G^{b} myeloid cells within fast- growing tumors compared with slow- growing tumors. Slow, n 8; fast, n 8. , $P <$ 0.001, Mann–Whitney test (bar mean SEM). G, Correlation between the proportion of CD11b^{b}Ly6G^{b} myeloid cells and tumor growth rate. n 19 (5 from sham, 14 from IR). PCC r 0.36, $P <$ 0.05.

H, Top, representative images of PD-L1 in slow- and fast-growing tumors. Bottom, quantification of the frequency of PD-L1^{b} cells in fast-growing tumors (n 8) com- pared with slow-growing tumors (n 8). , $P < 0.05$, Mann–Whitney test (bars, mean SEM). I, Top, representative images of TGFb in slow- and fast-growing tumors. Bottom, quantification of TGFb^{b} cells in fast- growing tumors (n 8) versus slow-growing tumors (n 8). , $P < 0.05$ Mann–Whitney test (bars, mean SEM). J, Top, representative images of pSMAD2 in slow- and fast- growing tumors. Bottom, quantification of pSMAD2^{b} cells in fast-growing tumors (n 8) compared with slow-growing tumors (n 8). , $P < 0.05$, Mann–Whitney test (bars, mean SEM). For H–J images, white arrows indicate cells zoomed in the image. Tan scale bars, 100 mm; green scale bars, 5 mm.

irradiated mice on the CAPE diet were predominantly infiltrated (80%), like the distribution obtained in sham-irradiated hosts.

We then examined the TME associated with tumors arising in irradiated hosts. CAPE inhibits the release of arachidonic acid from cell membranes, suppresses the enzyme activities of COX-1 and COX-2, and decreases COX-2 gene expression (53). Tumors from irradiated mice treated with CAPE exhibited decreased COX-2 (Fig. 6A), PD-L1^{b} cells (Fig. 6B), and CD11b^{b}GR1^{b} myeloid cells (Fig. 6C). In contrast, CD8^{b} TILs were increased (Fig. 6D). Consistent with host irradiation

acting via TGFb, tumors arising in irradiated CAPE-treated mice exhibited low TGFb and pSMAD2 (Fig. 6E and F). The altered immune composition of tumors arising in CAPE-treated, irradiated hosts was accompanied by increased apoptosis (Fig. 6G), concordant with their decreased growth rate compared with tumors arising in irradiated mice.

We next conducted RNA-seq of ER-negative tumors. We first sought to determine whether *Trp53*-null ER-negative tumors reflected the subtypes of human TNBC (54), using the TNBC type tool to assign subtype (33). We found that the subtypes of human TNBC were reflected in the spectrum of *Trp53*-null tumors. Although TNBC

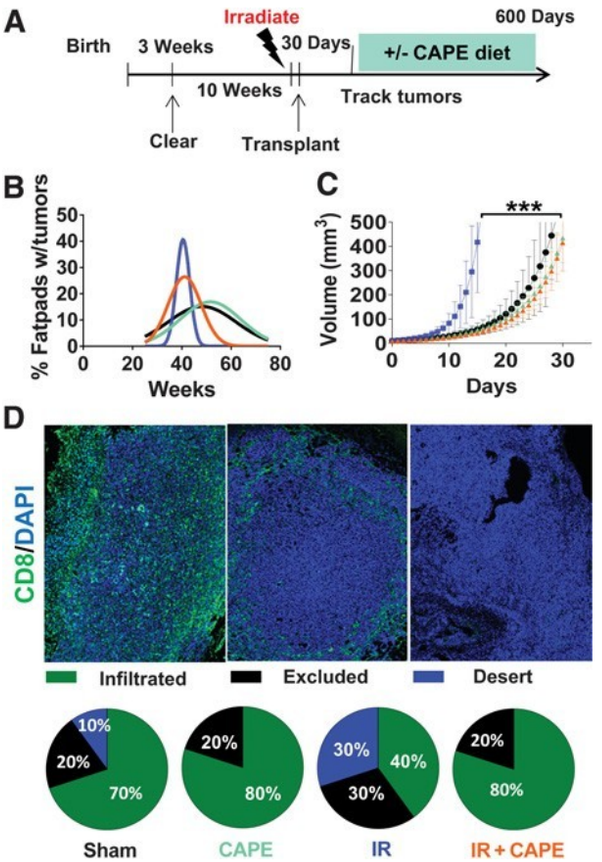

Figure 5.

CAPE prevents aggressive tumors from developing in irradiated hosts. A, Experimental scheme. The endogenous epithelium of the inguinal mammary glands of 3-week-old mice were surgically removed. Mice were aged until 10 weeks old, whole-body irradiated with 100 cGY SIR, and subsequently transplanted 3 days after irradiation with *Trp53*-null mammary fragments. Some mice received CAPE in their diet beginning 4 weeks after transplantation. Mice were monitored for tumorigenesis for ¼ approximately 600 days. B¼Percentage of palpable tumors detected over time for each treatment group. Sham, *n* 25 (black solid line); CAPE only, *n* 23 (green); irradiated (IR) only, *n* 20 (dark blue); IR ¼ CAPE, *n* 25 (orange). C, Tumor growth rate over 30 days for each treatment group. Mean SEM; sham (black), *n* 20; CAPE (green), *n* 20; IR (dark blue), *n* 19; IR CAPE (orange), *n* 22. , $P < 0.001$, one-way ANOVA. D, Tumors were classified into three lymphocytic infiltration pat- terns based on CD8^{þ} T-cell infiltrated (green), excluded (black), and desert (blue). IR (*n* ¼ 10), IR þ CAPE (*n* ¼ 10), sham (*n* ¼ 10), and CAPE (*n* ¼ 10).

subtype distribution varied by host treatment, the spectrum was not significantly different among treatment groups (Supplementary Fig. S2).

We then applied the immune gene expression cluster 2 (725 genes) identified from the microarray data (Fig. 6H). Tumors arising in irradiated mice clustered exclusively together in one arm of the dendrogram compared with tumors arising in sham, CAPE-treated and CAPE-treated, irradiated mice. Tumors arising in irradiated mice exhibited reduced cytokine and chemokine signaling necessary for antigen-presenting cell and T-cell migration and recruitment, as well as leukocyte activation. In comparison, tumors arising in CAPE- treated, irradiated mice were characterized by a significant reduction in overall inflammatory signaling and greater expression of antigen processing and presentation and leukocyte trafficking genes. To further assess these data, we examined a panel of previously published gene expression signatures that have been shown to measure aspects of immune signaling (28–32). These analyses demonstrated altered expression of both adaptive and innate immunity across treatment cohorts. Host irradiation resulted in tumors characterized by reduction ($P < 0.05$) of multiple signatures including T cells and T-cell– associated signatures (CD8, IL8, LCK), macrophages and macro- phage-associated signatures (CD68, M**j** Th1, M**j** CSF1, HCK), as well as neutrophil and natural killer cell signatures (CD44 and CD56) relative to sham-treated tumors (Fig. 6I; Supplementary Table S4). This shift in immune signaling was rescued by CAPE treatment of irradiated animals to levels present in tumors arising in control mice. CAPE alone did not appear to influence the immune TME. These data support host irradiation *per se* as the primary instigator of the immunosuppressive TME. Thus, treating mice with a dietary anti- inflammatory agent after radiation exposure prevented the consequences of host irradiation that drives aggressive tumors and an immunosuppressive TME.

Discussion

Here we used a model of *de novo* mammary carcinogenesis to show that host exposure to DIR or SIR at 10 months of age, which is roughly equivalent to middle-age in humans, promoted aggressive breast cancer characterized by rapid growth, an immunosuppressive TME, and sparse tumor-infiltrating lymphocytes. DIR, considered to be a more effective carcinogen than SIR, was significantly more effective in aged mice, suggesting an unexpected synergy between age and radi- ation quality. We focused on understanding the basis for the pro- nounced non-targeted radiation effect on rapid tumor growth rate, which is also evident in young irradiated hosts (15, 16). We found that only irradiated hosts gave rise to tumors lacking cytotoxic CD8^{þ} lymphocytes (i.e., immune deserts), and that the TME of fast-growing tumors was high in COX-2 and TGFb. These data suggested the hypothesis that host irradiation promotes inflammation and compro- mises systemic immune surveillance. To test whether compromised tumor immunity could be rescued, young mice were fed chow sup- plemented with CAPE, an anti-inflammatory and immunomodula- tory compound, after irradiation. Dietary CAPE prevented the development of rapidly growing, lymphocytic desert tumors, which was reflected in their transcriptomic rewiring. These data suggest that nonmutational radiation effects, particularly following DIR, were exacerbated in aged mice to fuel development of aggressive cancers by repressing antitumor immunity.

Although the possibility of a radiation-induced oncogenic mutation is widely believed to be the critical mechanism of carcinogenesis (55), human and experimental animal data suggest radiation exposure may activate or augment a cycle of subclinical inflammation and low-level tissue damage. Meanwhile, during the protracted evolution of cancer, the immune system concomitantly deteriorates with age, evidenced by increased proinflammatory cytokines, including TGFb, that are asso- ciated with increased risk of cancer (56, 57). Our studies suggest that these interact to drive aggressive cancer,

particularly following DIR. Radiation induces changes in cell phenotype and intercellular signaling that modify cell–cell interactions and the surrounding microenvironment, referred to as nontargeted effects (58). We devel- oped the mammary chimera model to evaluate whether host biology after exposure to radiation affects carcinogenesis. This model separates the effect of radiation on initiation, presumably via DNA damage and mutation, from those nonmutational mechanisms that may act on

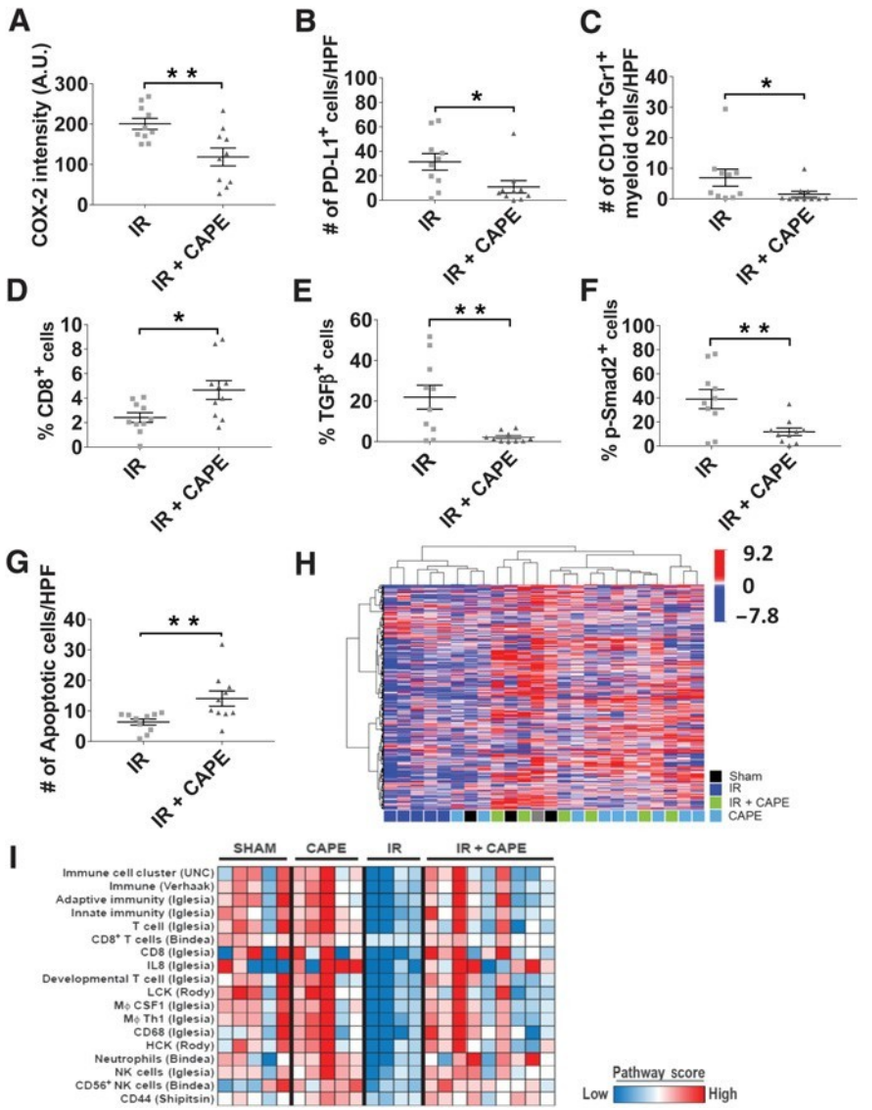

Figure 6.

CAPE prevents establishment of an immuno- suppressive TME. A–G, Immunofluorescence of tumors from irradiated (IR) and IR CAPE groups was compared. A, Quantification of COX-2 expression in tumors. B, The number of PD-L1^{+} cells per HPF in tumors. C, The number of CD11b^{+}Gr1^{+} cells per HPF in tumors. D, CD8^{+} T cells within tumors. TGFb^{+} cells (E) and pSMAD2^{+} cells (F) in tumors. G, Cell apoptosis was marked by cleaved caspase- 3^{+} cells per HPF in tumors. For A–G, each point is a mean of five random images from one tumor, IR: *n* = 10; IR CAPE: *n* = 10. *, $P < 0.05$; **, $P < 0.01$ by two-tailed *t* test or Mann–Whitney test (bars, mean ± SEM). H, Heatmap of differentially expressed immune genes. Sham (black, *n* = 3), IR (dark blue, *n* = 5), CAPE (light blue, *n* = 9), CAPE IR (green, *n* = 6). I, Panel of 18 gene expres- sion signatures comparing tumors from sham, CAPE, IR, and IR + CAPE treatments; red indicates high signature score, whereas blue corresponds with low signature score.

promotion. Cancers arising from *Trp53*-null outgrowths a year or more after host irradiation are more frequently ER-negative and metastatic and consistently grow more rapidly once detected compared to those arising in sham-irradiated mice (15, 16, 36). To ascertain the genetic contribution to cancer development following radiation, mice resistant to cancer development were crossed to sensitive mice, then backcrossed to generate genetically diverse mice that were used as hosts in the *Trp53*-null mammary chimera model (35). Bioinformatics analysis of the genetic loci associated with tumor latency in irradiated mice identified enrichment for genes involved in immune response, including signaling pathways of natural killer cells and cytokines. Consistent with this, plasma levels of certain cytokines in irradiated mice are significantly associated with tumor latency. Analysis of the candidate genes within these loci identified TGFb as a critical upstream regulator in irradiated mice, consistent with our prior studies using *Tgfb1*$^{+/-}$ hosts (16). Our studies in aged mice confirmed that TGFb is an important mediator of radiation-carcinogenesis.

Correlative analysis of the tumor phenotypes and TME showed that lack of lymphocytic infiltrate was associated with rapid tumor growth

rate. Subsequent expression profiling and prior literature led to the hypothesis that low-dose radiation exposure compromises antitumor immunity, but the exact nature of the immune changes is insufficiently clear. Although cell-type depletion studies could lend further support, our model, in which tumors arise after 12 to 18 months, makes this approach very challenging. Depletion of a specific cell type (e.g. CD4 or CD8) with specific antibodies to cell surface markers is widely used but would not be feasible for the duration of the experiment, nor can they be timed to coincide with a specific event because tumors arise spontaneously.

Dietary anti-inflammatory CAPE abrogated the effect of host irradiation that promoted aggressive tumors. CAPE inhibits cyto- kine and chemokine production, the proliferation of T cells, and lymphokine production, suppresses the inflammatory process, and is a potent and a specific inhibitor of NFkB activation (17). Mech- anistically, CAPE has been shown to exhibit its anti-inflammatory effects by being the most potent modulator of arachidonic acid cascade through the inhibition of leukotriene production and prostaglandin formation by inhibiting COX and lipoxygenase

pathways. COX-2 may be a critical factor in allowing cancer cells to escape host immune defenses by modulation of cytokine produc- tion, dysfunction of dendritic cells, and suppression of lymphocyte proliferation associated with immunosuppression and tumorigen-

esis (59). Consistent with this, COX-2 was significantly upregulated in tumors arising from irradiated hosts but when treated with CAPE, the suppressive immune signature was reversed, and

COX-2 expression significantly decreased.

We observed an inverse relationship between COX-2 and CD8^{þ}

T-cell infiltration. High TILs is a favorable prognostic factor in certain breast cancer subtypes (60). COX-2 inhibition in mice accelerates accumulation of cytotoxic T cells within tumors and consequently slows tumor growth (61). Our data suggested that these cytotoxic TILs were reactive, albeit insufficient to eliminate tumors, as evidenced by slower tumor growth. COX-2 expression negatively correlated with TILs in fast-growing tumors, as was PD-L1; both were abrogated in CAPE-fed mice. CAPE treatment of irradiated hosts significantly decreased subsequent tumor growth rate and increased apoptosis, consistent with the observed increased TILs. CAPE treatment only affected these parameters in tumors arising from the irradiated hosts.

In conclusion, these data show that ionizing radiation generates mammary cancers in aged mice that are more aggressive and char- acterized by an immunosuppressive TME. Although radiation quality and age appear to particularly synergize, this biology was evident in young mice in which dietary intervention with CAPE mitigated radiation's systemic effects. The concept that establishment of an immunosuppressive TME fuels radiation carcinogenesis adds cre- dence to the use of anti-inflammatory agents in breast cancer pre- vention. Further support is given to this idea by the current ongoing clinical trial using aspirin as an adjuvant therapy for breast cancer (NCT02927249).

Disclosure of Potential Conflicts of Interest

No potential conflicts of interest were disclosed.

Authors' Contributions

Conception and design: C. Omene, L. Ma, M.H. Barcellos-Hoff Development of methodology: C. Omene, L. Ma, I. Illa-Bochaca Acquisition of data (provided animals, acquired and managed patients, provided facilities, etc.): C. Omene, L. Ma, H. Ouyang, I. Illa-Bochaca, M.S. Patel, S. Demaria Analysis and interpretation of data (e.g., statistical analysis, biostatistics, computational analysis): C. Omene, L. Ma, J. Moore, H. Ouyang, I. Illa-Bochaca,

C. Sebastiano, J.-H. Mao, K. Karagoz, M.L. Gatza, M.H. Barcellos-Hoff Writing, review, and/or revision of the manuscript: C. Omene, L. Ma, J. Moore,

H. Ouyang, M.S. Patel, S. Demaria, K. Karagoz, M.L. Gatza, M.H. Barcellos-Hoff Administrative, technical, or material support (i.e., reporting or organizing data, constructing databases): C. Omene, L. Ma, J. Moore, I. Illa-Bochaca, W. Chou Study supervision: C. Omene, M.L. Gatza, M.H. Barcellos-Hoff

Acknowledgments

The authors would like to acknowledge expert assistance from Trevor Jones, Xiaolu Li, and Derek Francis. We thank the faculty and staff of the NASA Space Research Laboratory at Brookhaven National Laboratory for beamline support and members of the NYUMC Laura and Isaac Perlmutter Cancer Center Genome Technology Center. This research was supported by NASA Specialized Center for Research in Radiation Health Effects, NNX09AM52G at New York University School of Medicine, and NIH R01CA190980 and R01CA19098005S1 awards at University of California, San Francisco (to M.H. Barcellos-Hoff) and K08 CA172722 (to C. Omene).

The costs of publication of this article were defrayed in part by the payment of page charges. This article must therefore be hereby marked *advertisement* in accordance with 18 U.S.C. Section 1734 solely to indicate this fact.

Received April 9, 2019; revised July 26, 2019; accepted November 27, 2019;
published first December 12, 2019.

References

1. Barcellos-Hoff MH, Lyden D, Wang TC. The evolution of the cancer niche during multistage carcinogenesis. Nat Rev Cancer 2013;13:511–8.
2. Ronckers CM, Erdmann CA, Land CE. Radiation and breast cancer: a review of current evidence. Breast Cancer Res 2005;7:21–32.
3. Medzhitov R. Inflammation 2010: new adventures of an old flame. Cell 2010;140: 771–6.
4. Grivennikov SI, Greten FR, Karin M. Immunity, inflammation, and cancer. Cell 2010;140:883–99.
5. Mittal D, Gubin MM, Schreiber RD, Smyth MJ. New insights into cancer immunoediting and its three component phases-elimination, equilibrium and escape. Curr Opin Immunol 2014;27:16–25.
6. Schreiber RD, Old LJ, Smyth MJ. Cancer immunoediting: integrating immunity's roles in cancer suppression and promotion. Science 2011; 331:1565–70.
7. Berrington de Gonzalez A, Curtis RE, Kry SF, Gilbert E, Lamart S, Berg CD, et al. Proportion of second cancers attributable to radiotherapy treatment in adults: a cohort study in the US SEER cancer registries. Lancet Oncol 2011; 12:353–60.
8. Bhatia S, Robison LL, Oberlin O, Greenberg M, Bunin G, Fossati-Bellani F, et al. Breast cancer and other second neoplasms after childhood Hodgkin's disease. N Engl J Med 1996;334:745–51.
9. Moskowitz CS, Chou JF, Wolden SL, Bernstein JL, Malhotra J, Novetsky Friedman D, et al. Breast cancer after chest radiation therapy for childhood cancer. J Clin Oncol 2014;32:2217–23.
10. Castiglioni F, Terenziani M, Carcangiu ML, Miliano R, Aiello P, Bertola L, et al. Radiation effects on development of HER2-positive breast carcinomas. Clin Cancer Res 2007;13:46–51.
11. Horst KC, Hancock SL, Ognibene G, Chen C, Advani RH, Rosenberg SA, et al. Histologic subtypes of breast cancer following radiotherapy for Hodgkin lym- phoma. Ann Oncol 2014;25:848–51.

12. Sarkar D, Fisher PB. Molecular mechanisms of aging-associated inflammation. Cancer Lett 2006;236:13–23.
13. Hayashi T, Kusunoki Y, Hakoda M, Morishita Y, Kubo Y, Maki M, et al. Radiation dose-dependent increases in inflammatory response markers in A- bomb survivors. Int J Radiat Biol 2003;79:129–36.
14. Harman D. Aging: a theory based on free radical and radiation chemistry. J Gerontol 1956;11:298–300.
15. Illa-Bochaca I, Ouyang H, Tang J, Sebastiano C, Mao J-H, Costes SV, et al. Densely ionizing radiation acts via the microenvironment to promote aggressive Trp53 null mammary carcinomas. Cancer Res 2014;74:7137–48.
16. Nguyen DH, Oketch-Rabah HA, Illa-Bochaca I, Geyer FC, Reis-Filho JS, Mao JH, et al. Radiation acts on the microenvironment to affect breast carcinogenesis by distinct mechanisms that decrease cancer latency and affect tumor type. Cancer Cell 2011;19:640–51.
17. Armutcu F, Akyol S, Ustunsoy S, Turan FF. Therapeutic potential of caffeic acid phenethyl ester and its anti-inflammatory and immunomodulatory effects (review). Exp Ther Med 2015;9:1582–8.
18. Harvey JM, Clark GM, Osborne CK, Allred DC. Estrogen receptor status by immunohistochemistry is superior to the ligand-binding assay for predicting response to adjuvant endocrine therapy in breast cancer. J Clin Oncol 1999;17: 1474–81.
19. Carvalho BS, Irizarry RA. A framework for oligonucleotide microarray pre- processing. Bioinformatics 2010;26:2363–7.
20. Gautier L, Cope L, Bolstad BM, Irizarry RA. affy–analysis of Affymetrix GeneChip data at the probe level. Bioinformatics 2004;20:307–15.
21. Zhao Y, Simon R. BRB-ArrayTools Data Archive for human cancer gene expres- sion: a unique and efficient data sharing resource. Cancer Inform 2008;6:9–15.
22. Parker JS, Mullins M, Cheang MC, Leung S, Voduc D, Vickery T, et al. Supervised risk predictor of breast cancer based on intrinsic subtypes. J Clin Oncol 2009;27: 1160–7.

23. Kim D, Pertea G, Trapnell C, Pimentel H, Kelley R, Salzberg SL. TopHat2: accurate alignment of transcriptomes in the presence of insertions, deletions and gene fusions. Genome Biol 2013;14:R36.
24. Love MI, Huber W, Anders S. Moderated estimation of fold change and dispersion for RNA-seq data with DESeq2. Genome Biol 2014;15: 550.
25. Subramanian A, Tamayo P, Mootha VK, Mukherjee S, Ebert BL, Gillette MA, et al. Gene set enrichment analysis: a knowledge-based approach for interpreting genome-wide expression profiles. PNAS 2005;102:15545–50.
26. Zhang B, Kirov S, Snoddy J. WebGestalt: an integrated system for exploring gene sets in various biological contexts. Nucleic Acids Res 2005;33(Web Server issue): W741–8.
27. Wang J, Duncan D, Shi Z, Zhang B. WEB-based GEne SeT AnaLysis Toolkit (WebGestalt): update 2013. Nucleic Acids Res 2013;41(Web Server issue): W77–83.
28. Iglesia MD, Parker JS, Hoadley KA, Serody JS, Perou CM, Vincent BG. Genomic analysis of immune cell infiltrates across 11 tumor types. J Natl Cancer Inst 2016;108. doi: 10.1093/jnci/djw144.
29. Bindea G, Mlecnik B, Tosolini M, Kirilovsky A, Waldner M, Obenauf AC, et al. Spatiotemporal dynamics of intratumoral immune cells reveal the immune landscape in human cancer. Immunity 2013;39:782–95.
30. Shipitsin M, Campbell LL, Argani P, Weremowicz S, Bloushtain-Qimron N, Yao J, et al. Molecular definition of breast tumor heterogeneity. Cancer Cell 2007;11: 259–73.
31. Yoshihara K, Shahmoradgoli M, Martinez E, Vegesna R, Kim H, Torres-Garcia W, et al. Inferring tumour purity and stromal and immune cell admixture from expression data. Nat Commun 2013;4:2612.
32. Fan C, Prat A, Parker JS, Liu Y, Carey LA, Troester MA, et al. Building prognostic models for breast cancer patients using clinical variables and hundreds of gene expression signatures. BMC Med Genet 2011;4:3.
33. Chen X, Li J, Gray WH, Lehmann BD, Bauer JA, Shyr Y, et al. TNBCtype: a subtyping tool for triple-negative breast cancer. Cancer Inform 2012;11: 147–56.
34. Jerry DJ, Kittrell FS, Kuperwasser C, Laucirica R, Dickinson ES, Bonilla PJ, et al. A mammary-specific model demonstrates the role of the p53 tumor suppressor gene in tumor development. Oncogene 2000;19:1052–8.
35. Zhang P, Lo A, Huang Y, Huang G, Liang G, Mott J, et al. Identification of genetic loci that control mammary tumor susceptibility through the host microenvi- ronment. Sci Rep 2015;5:8919.
36. Tang J, Fernandez-Garcia I, Vijayakumar S, Martinez-Ruiz H, Illa-Bochaca I, Nguyen DH, et al. Irradiation of juvenile, but not adult, mammary gland increases stem cell self-renewal and estrogen receptor negative tumors. Stem Cells 2013;32:649–61.
37. Herschkowitz JI, Simin K, Weigman VJ, Mikaelian I, Usary J, Hu Z, et al. Identification of conserved gene expression features between murine mammary carcinoma models and human breast tumors. Genome Biol 2007;8:R76.
38. Nguyen DH, Fredlund E, Zhao W, Perou CM, Balmain A, Mao J-H, et al. Murine microenvironment metaprofiles associate with human cancer etiology and intrinsic subtypes. Clin Cancer Res 2013;19:1353–62.
39. Onder TT, Gupta PB, Mani SA, Yang J, Lander ES, Weinberg RA. Loss of E- cadherin promotes metastasis via multiple downstream transcriptional path- ways. Cancer Res 2008;68:3645–54.
40. Andarawewa KL, Erickson AC, Chou WS, Costes SV, Gascard P, Mott JD, et al. Ionizing radiation predisposes nonmalignant human mammary epithelial cells to undergo transforming growth factor b induced epithelial to mesenchymal transition. Cancer Res 2007;67:8662–70.
41. Lee J, Son MJ, Woolard K, Donin NM, Li A, Cheng CH, et al. Epigenetic- mediated dysfunction of the bone morphogenetic protein pathway inhibits differentiation of glioblastoma-initiating cells. Cancer Cell 2008;13:69–80.
42. Yan G, Zhao H, Zhang Q, Zhou Y, Wu L, Lei J, et al. A RIPK3-PGE2 circuit mediates myeloid-derived suppressor cell-potentiated colorectal carcinogenesis. Cancer Res 2018;78:5586–99.
43. Hegde PS, Karanikas V, Evers S. The where, the when, and the how of immune monitoring for cancer immunotherapies in the era of checkpoint inhibition. Clin Cancer Res 2016;22:1865–74.
44. Bercovici N, Trautmann A. Revisiting the role of T cells in tumor regression. Oncoimmunology 2012;1:346–50.
45. Terabe M, Matsui S, Park JM, Mamura M, Noben-Trauth N, Donaldson DD, et al. Transforming growth factor-b production and myeloid cells are an effector mechanism through which CD1d-restricted T cells block cytotoxic T lympho- cyte-mediated tumor immunosurveillance: abrogation prevents tumor recur- rence. J Exp Med 2003;198:1741–52.
46. Liu CY, Wang YM, Wang CL, Feng PH, Ko HW, Liu YH, et al. Population alterations of L-arginase- and inducible nitric oxide synthase-expressed $CD11b^{b}/CD14^{-}/CD15^{b}/CD33^{b}$ myeloid-derived suppressor cells and $CD8^{b}$ T lymphocytes in patients with advanced-stage non-small cell lung cancer. J Cancer Res Clin Oncol 2010;136:35–45.
47. Amarnath S, Mangus CW, Wang JC, Wei F, He A, Kapoor V, et al. The PDL1- PD1 axis converts human TH1 cells into regulatory T cells. Sci Transl Med 2011; 3:111ra20.
48. Prima V, Kaliberova LN, Kaliberov S, Curiel DT, Kusmartsev S. COX2/mPGES1/ PGE2 pathway regulates PD-L1 expression in tumor-associated macrophages and myeloid-derived suppressor cells. Proc Natl Acad Sci U S A 2017;114: 1117–22.
49. Gonzalez-Junca A, Driscoll K, Pellicciotta I, Du S, Lo CH, Roy R, et al. Autocrine TGFbeta is a survival factor for monocytes and drives immunosuppressive lineage commitment. Cancer Immunol Res 2019;7:306–20.
50. Hearps AC, Martin GE, Angelovich TA, Cheng W-J, Maisa A, Landay AL, et al. Aging is associated with chronic innate immune activation and dysregulation of monocyte phenotype and function. Aging Cell 2012;11:867–75.
51. Omene C, Wu J, Frenkel K. Caffeic acid phenethyl ester (CAPE) derived from propolis, a honeybee product, inhibits growth of breast cancer stem cells. Invest New Drugs 2011;30:1279–88.
52. Wu J, Omene C, Karkoszka J, Bosland M, Eckard J, Klein CB, et al. Caffeic acid phenethyl ester (CAPE), derived from a honeybee product propolis, exhibits a diversity of anti-tumor effects in pre-clinical models of human breast cancer. Cancer Lett 2011;308:43–53.
53. Sud'ina GF, Mirzoeva OK, Pushkareva MA, Korshunova GA, Sumbatyan NV, Varfolomeev SD. Caffeic acid phenethyl ester as a lipoxygenase inhibitor with antioxidant properties. FEBS Lett 1993;329:21–4.
54. Lehmann BD, Bauer JA, Chen X, Sanders ME, Chakravarthy AB, Shyr Y, et al. Identification of human triple-negative breast cancer subtypes and preclinical models for selection of targeted therapies. J Clin Invest 2011;121: 2750–67.
55. United National Scientific Committee on the Effects of Atomic Radiation. Sources and effects of ionizing radiation. UNSCEAR 2008 report to the General Assembly with scientific annexes. Vol. 1. New York: United Nations; 2008. Available from: http://www.unscear.org/docs/reports/2008/09-86753_Report_2008_Annex_B.pdf.
56. Krieglstein K, Miyazono K, ten Dijke P, Unsicker K. TGF-beta in aging and disease. Cell Tissue Res 2012;347:5–9.
57. Bianchi-Frias D, Vakar-Lopez F, Coleman IM, Plymate SR, Reed MJ, Nelson PS. The effects of aging on the molecular and cellular composition of the prostate microenvironment. PLoS One 2010;5:e12501.
58. Wright EG, Coates PJ. Untargeted effects of ionizing radiation: Implications for radiation pathology. Mutation Res 2006;597:119–32.
59. Hashemi Goradel N, Najafi M, Salehi E, Farhood B, Mortezaee K. Cyclooxy- genase-2 in cancer: a review. J Cell Physiol 2019;234:5683–99.
60. Denkert C, von Minckwitz G, Darb-Esfahani S, Lederer B, Heppner BI, Weber KE, et al. Tumour-infiltrating lymphocytes and prognosis in different subtypes of breast cancer: a pooled analysis of 3771 patients treated with neoadjuvant therapy. Lancet Oncol 2018;19:40–50.
61. DeLong P, Tanaka T, Kruklitis R, Henry AC, Kapoor V, Kaiser LR, et al. Use of cyclooxygenase-2 inhibition to enhance the efficacy of immunotherapy. Cancer Res 2003;63:7845–52.